HHS Public Access

Author manuscript

Biochim Biophys Acta Mol Cell Biol Lipids. Author manuscript; available in PMC 2019 October 01.

Published in final edited form as:

Biochim Biophys Acta Mol Cell Biol Lipids. 2019 October ; 1864(10): 1269–1279. doi:10.1016/j.bbalip.2019.06.004.

Multiple neurosteroid and cholesterol binding sites in voltage-dependent anion channel-1 determined by photo-affinity labeling

Wayland W.L. Cheng[a,1], **Melissa M. Budelier**[a,b,1], **Yusuke Sugasawa**[a], **Lucie Bergdoll**[f], **María Queralt-Martín**[h], **William Rosencrans**[h], **Tatiana K. Rostovtseva**[h], **Zi-Wei Chen**[a,e], **Jeff Abramson**[f], **Kathiresan Krishnan**[c], **Douglas F. Covey**[a,c,d,e], **Julian P. Whitelegge**[g], **Alex S. Evers**[a,c,d,e,*]

[a]Department of Anesthesiology, Washington University in St. Louis, MO 63110, USA

[b]Department of Biochemistry and Molecular Biophysics, Washington University in St. Louis, MO 63110, USA

[c]Department of Developmental Biology, Washington University in St. Louis, MO 63110, USA

[d]Department of Psychiatry, Washington University in St. Louis, MO 63110, USA

[e]Taylor Family Institute for Innovative Psychiatric Research, Washington University in St. Louis, MO 63110, USA

[f]Department of Physiology, David Geffen School of Medicine at UCLA, Los Angeles, CA 90095, USA

[g]Department of Psychiatry and Biobehavioral Sciences, David Geffen School of Medicine at UCLA, Los Angeles, CA 90095, USA

[h]Section on Molecular Transport, Eunice Kennedy Shriver National Institute of Child Health and Human Development, National Institutes of Health, Bethesda, MD 20892, USA

Abstract

Voltage-dependent anion channel-1 (VDAC1) is a mitochondrial porin that is implicated in cellular metabolism and apoptosis, and modulated by numerous small molecules including lipids. VDAC1 binds sterols, including cholesterol and neurosteroids such as allopregnanolone. Biochemical and computational studies suggest that VDAC1 binds multiple cholesterol molecules, but photolabeling studies have identified only a single cholesterol and neurosteroid binding site at E73. To identify all the binding sites of neurosteroids in VDAC1, we apply photo-affinity labeling using two sterol-based photolabeling reagents with complementary photochemistry: 5α-6-AziP which contains an aliphatic diazirine, and KK200 which contains a trifluoromethyl-

*Corresponding author at: Department of Anesthesiology, Washington University School of Medicine, Campus Box 8054, St. Louis, MO 63110, USA. eversa@wustl.edu (A.S. Evers).

[1]Wayland W. L. Cheng and Melissa M. Budelier contributed equally to this work.

Supplementary data to this article can be found online at https://doi.org/10.1016/j.bbalip.2019.06.004.

Transparency document

The Transparency document associated with this article can be found, in online version.

Declaration of Competing Interest

The authors declare no competing interests.

phenyldiazirine (TPD) group. 5α-6-AziP and KK200 photolabel multiple residues within an E73 pocket confirming the presence of this site and mapping sterol orientation within this pocket. In addition, KK200 photolabels four other sites consistent with the finding that VDAC1 co-purifies with five cholesterol molecules. Both allopregnanolone and cholesterol competitively prevent photolabeling at E73 and three other sites indicating that these are common sterol binding sites shared by both neurosteroids and cholesterol. Binding at the functionally important residue E73 suggests a possible role for sterols in regulating VDAC1 signaling and interaction with partner proteins.

Keywords

Neurosteroid; Cholesterol; Voltage-dependent anion channel (VDAC); Protein drug interaction; Photoaffinity labeling; Mass spectrometry

1. Introduction

Voltage-dependent anion channel-1 (VDAC1) is a β-barrel integral membrane protein residing in the mitochondrial outer membrane that forms a pore for the transport of ions and small molecules and is also thought to play a role in apoptosis [1]. The function of this porin is regulated by numerous factors including membrane potential [2], calcium [3,4], proteins [5–8], small molecule ligands [9], and lipids [10]. Sterols are an important class of membrane lipids, which include cholesterol and neurosteroids, both of which have been shown to bind to VDAC1 [11–16]. Cholesterol may play a role in modulating VDAC1 function [17], although basic channel properties such as conductance and gating are not affected [18]; whether neurosteroids alter VDAC1 function is not known. Moreover, the sites of sterol binding in VDAC1 have not been fully delineated.

The structural basis of cholesterol and neurosteroid binding to VDAC1 has been the subject of several studies. Detergent-solubilized bovine VDAC1 co-purifies with an estimated five cholesterol molecules per protein [19], and NMR chemical shift data suggest multiple cholesterol binding sites [13]. Subsequently, five putative cholesterol binding sites have been proposed using docking and molecular dynamics simulations [14]. To experimentally map sterol binding to VDAC1, we previously employed photo-affinity labeling using cholesterol and neurosteroid-based reagents, and identified a single binding pocket centered at E73 [11,12]. Sterol binding to this site is of potential functional significance, since E73 has been implicated in VDAC1-mediated apoptosis through hexokinase binding [20], and VDAC1 dimerization [21]. However, E73 was not identified as a sterol binding site in the aforementioned NMR or computational studies.

To resolve this apparent discrepancy, we performed a photo-affinity labeling study using multiple sterol-based reagents with complementary photochemistry to more comprehensively map sterol binding sites in VDAC1. By doing so, we substantiate the presence of a sterol binding pocket adjacent to E73 that can be occupied by either cholesterol or the neurosteroid, allopregnanolone, and map neurosteroid binding orientation within this site. In addition, we identify four other binding sites also shared by cholesterol and allopregnanolone. While allopregnanolone alike to cholesterol does not significantly

alter the gating properties of VDAC1, our results raise the hypothesis that neurosteroids and cholesterol may modulate other functional properties of VDAC1 by binding to common sites.

2. Material and methods

2.1. Expression and purification of mVDAC1 from E. coli

Mouse VDAC1 was expressed and purified as previously described [22]. The mVDAC1 E73A and E73Q mutants were generated using Stratagene's QuikChange site-directed mutagenesis kit (La Jolla, CA), and expressed and purified the same way as WT protein.

2.2. Synthesis of neurosteroid photolabeling reagents

The synthesis of 5α-6-AziP and KK200 were described in detail previously [23].

2.3. Top-down MS of photolabeled mVDAC1

80 μg of WT or E73Q mVDAC1 was reconstituted in bicelles by adding a 35% solution of DMPC/CHAPSO bicelles (4:1 v/v protein:bicelles), and incubating on ice for 30 min. Samples were then diluted to 100 μL with 20 mM Tris buffer pH 8, and photolabeled in a quartz cuvette with > 320 nm UV light. For top-down MS analysis, samples were then reduced, precipitated [24], reconstituted in formic acid and chloroform/methanol/water 4:4:1, and analyzed on a Thermo Orbitrap Elite MS as previously described [11]. Full spectra of intact photo-labeled mVDAC1 were acquired on the LTQ. HCD fragmentation spectra of the 31+ charge state were acquired at 60,000 resolution and normalized energy of 10. Deconvolution of full spectra from the LTQ was performed using MagTran [25]. MASH was used to analyze top-down HCD fragmentation data [26]. Each identified fragment ion was manually verified and accepted if within 10 ppm of predicted.

2.4. Bottom-up MS of mVDAC1 photolabeled with 5α-6-AziP or KK200

30 μg aliquots of mVDAC1 photolabeled with 5α-6-AziP from top-down MS experiments were precipitated with a 2D-SDS clean-up kit (GE healthcare), solubilized in 5% Rapigest™ and 8 M urea, precipitated again, and re-solubilized in 8 M urea, 0.2% Rapigest™. After reduction with 5 mM triscarboxyethlyphosphine (TCEP) and alkylation with 5 mM idoacetamide, the samples were diluted to a final urea concentration of 1 M, and digested overnight with 2 μg trypsin. Digestions were stopped with 1% formic acid (FA), and peptides were sequentially extracted with C4 and C18 stage tips. Peptides were eluted from stage tips with 10% acetonitrile (CAN), 1% FA, dried via vacuum centrifugation, resuspended in 10% ACN, 1% FA, and analyzed by LC/MS/MS on an Orbitrap Elite MS. For KK200 labeling and experiments using either 5α-6-AziP or KK200 to assess competitive prevention of photo-labeling by allopregnanolone and cholesterol, mVDAC1 samples were photolabeled in 0.1% lauryldimethylamine-N-oxide (LDAO). In the case of 5α-6-AziP, no difference in the efficiency or site of labeling (E73) was observed between bicelles and detergent. Photolabeling in LDAO enabled direct analysis of sample digests making relative quantification of unlabeled and labeled peptides feasible. After photolabeling, these samples were buffer exchanged using Biospin6 columns (Biorad) preequilibrated with 50 mM triethylammonium bicarbonate (TEABC) (pH 7.5) and 0.05%

LDAO. The samples were then reduced and alkylated with 5 mM TCEP, 5 mM N-ethylmaleimide, followed by 2 mM dithiothreitol (DTT). Digestion was initiated by adding 10 μg of trypsin at 37 °C overnight, and then directly analyzed by LC-MS/MS analysis using a home-made PLRP-S column [23] coupled to an Orbitrap Elite MS. LC-MS/MS used a 1–90% ACN gradient, and top-20 data-dependent acquisition scans using collision-induced dissociation (CID) or higher-energy collision dissociation (HCD).

The data were searched for photolabeled peptides using PEAKS software with 20 ppm and 0.1 Da mass accuracy for precursor peptides and fragment ions, respectively. Photolabeled peptides were then manually verified and only accepted if: 1) the peptide is tryptic, and 2) the corresponding non-photolabeled peptide eluted earlier in the LC gradient than the photolabeled peptide. MS2 spectra of each photo-labeled peptide were then manually assigned using a mass accuracy limit of 20 ppm. Photolabeling efficiency was calculated by determining the area under the curve of extracted ion chromatograms for photo-labeled and non-photolabeled peptides. Statistical analysis for 5α-6-AziP and KK200 competition experiments were performed using a paired *t*-test and one-way ANOVA (Tukey's HSD).

2.5. Docking simulations

Docking of allopregnanolone or KK200 to mVDAC1 was performed using AutoDock 4.2 [27]. The mVDAC1 template was prepared using PDB 3emn in AutoDock Tools. The structure of KK200 was generated using Maestro (Academic version, Schrodinger) using the 2D draw and 3D conversion function, after which Gasteiger charges and free torsion angles were determined by AutoDock Tools. Docking simulations of KK200 were prepared using a grid box with dimensions 22 Å × 22 Å × 28 Å centered around E73, with 1 Å grid spacing, and 1000 runs were performed using a genetic algorithm. For docking of allopregnanolone and cholesterol, a box size of 16 Å × 16 Å × 13 Å with 0.3 Å grid spacing was used. Results were clustered using a 2 Å RMSD. Two clusters of poses were identified for allopregnanolone and cholesterol within the binding groove formed by E73, Y62, and F99.

2.6. mVDAC1 and Gramicidin A reconstitution in planar lipid bilayers and current recordings

Planar lipid membranes were formed from two opposing lipid monolayers across 70–90 μm diameter orifice in the 15 μm-thick Teflon partition separating two ~1.5 ml compartments as previously described [10]. Lipid bilayers were made from soybean polar lipid extract (Avanti Polar Lipids, Inc) in pentane. Channel insertion was achieved by adding 0.5–2 μL of mVDAC1 stock solution (5 mg/ml in 10 mM Tris, 100 mM NaCl, 0.1% LDAO) into the aqueous phase of 1 M KCl buffered with 5 mM HEPES at pH 7.4 in the *cis* compartment while stirring. The potential was defined as positive when it was greater at the side of mVDAC1 addition (*cis*-side). Current recordings were performed as described previously [10] using an Axopatch 200B amplifier (Axon Instruments, Inc.) in the voltage clamp mode. The voltage-dependent properties of an mVDAC1-containing membrane were assessed following the previously devised protocol [2,10] in which gating is inferred from the channels response to a symmetrical 5 mHz triangular voltage wave with ± 60 mV amplitude from a Function Waveform Generator 33220A (Hewlett Packard). Data were acquired with a Digidata 1440A board (Axon Instruments Inc.) at a sampling frequency of 2 Hz and

analyzed using the pClamp 10.7 software (Axon Instruments, Inc.). Analysis of VDAC voltage-gating was performed following published protocols [10,28]. In each experiment, current records were collected on multichannel membranes in response to 5–10 periods of triangular voltage waves. Only the part of the wave during which the channels were reopening was used for the subsequent analysis. Given the variable number of channels per experiment, the average conductance (G) was normalized to the maximum conductance (G_{max}).After current records of 20 to 850 channels were recorded, the aliquots of allopregnanolone in 10 or 50 mM stock solution in ethanol were added to the buffer solutions at the both sides of the membrane. The records were taken 10 min after each allopregnanolone addition. For gramicidin A measurements, gramicidin A was added from 1 nM ethanol solutions to both sides of the membrane as previously described [10]. Gramicidin A was a generous gift from O. S. Andersen (Cornell University Medical College). Single-channel gramicidin A measurements were performed in the voltage clamp mode at +100 mV. The signal was filtered by a low-pass Bessel filter at 1 kHz, then digitally filtered at 500 Hz using a Bessel algorithm in Clampfit 10.3. Channel lifetimes were calculated by fitting logarithmic exponentials to logarithmically binned histograms. The mean number of events for each experiment was 250 to 2500. All lifetime histograms used 10 bins per decade.

3. Results

3.1. The neurosteroid photolabeling reagent, 5α-6-AziP, labels E73 in mVDAC1

To map sterol binding sites in VDAC1, murine VDAC1 (mVDAC1) was expressed and purified from *E. coli*, re-folded from inclusion bodies, and reconstituted in DMPC/CHAPSO bicelles as previously described [22,29]. mVDAC1 was then was photolabeled with two reagents based on the endogenous neurosteroid, allopregnanolone: 3α,5α-6-azi-pregnanolone (5α-6-AziP), and a 3α,5α-pregnanolone compound with a trifluoromethylphenyl-diazirine (TPD) in the 17-position (KK200) (Fig. 1A). These reagents were previously used to map neurosteroid binding sites in pentameric ligand-gated ion channels [23,30], and have complementary characteristics. 5α-6-AziP has an aliphatic diazirine in the 6-position; this compound more closely resembles allopregnanolone, but preferentially photolabels nucleophilic side chains such as glutamate and tyrosine. KK200 has a TPD group, which is bulkier, but is expected to form a reactive carbene that will covalently modify any nearby amino acid. The TPD group also adds a lengthy hydrophobic moiety to the steroid such that the labeled residue is ~6–7 Å from the steroid backbone. Thus, KK200 has more favorable photochemistry, is more likely to label all sterol binding sites, and facilitates mapping of sterol binding orientation within a site.

We first photolabeled mVDAC1 with 5α-6-AziP. To determine the efficiency and stoichiometry of labeling, we performed an exhaustive labeling protocol (photolabeling performed three times with 100 μM 5α-6-AziP added each time), and analyzed the labeled protein by intact protein MS using a Thermo Orbitrap Elite mass spectrometer [23]. Analysis of non-photolabeled mVDAC1 shows a peak corresponding to intact, unmodified His-tagged mVDAC1 (Fig. 1A). After photolabeling with 5α-6-AziP, the mass of mVDAC1 shifts 316 Da corresponding to mVDAC1 labeled with one 5α-6-AziP (Fig. 1A). Under this

exhaustive photolabeling condition, mVDAC1 is photolabeled with > 97% efficiency, and the spectrum is dominated by a single-labeled mVDAC1 species with only a tiny double-labeled species (Fig. 1A). This indicates that 5α-6-AziP predominantly photolabels mVDAC1 at a single site.

Top-down fragmentation of the mVDAC1 species photolabeled with one 5α-6-AziP using higher energy collision dissociation (HCD) shows a series of *b* ions that localize the photolabeled site to an N-terminal region from S43-E120 (Fig. 1B). To identify the exact photolabeled residue, tryptic digests of photolabeled mVDAC1 were analyzed by LCMS/MS using collision-induced dissociation (CID). This revealed a single tryptic peptide photolabeled at E73 (Fig. 1C, Table 1). E73 is uniquely positioned in the transmembrane domain of β-strand 4 facing out into the membrane (Fig. 2E) [22]. Efficient singular labeling of E73 by 5α-6-AziP may be driven by the photochemical preference of aliphatic diazirines for the nucleophilic glutamate side chain. We previously showed that E73 has a pKa of approximately 7 [21]. To test whether 5α-6-AziP is labeling the de-protonated E73 side chain, we photolabeled mVDAC1 at pH 8 and pH 6, and analyzed the samples using intact protein MS. Changing the pH from 8 to 6 significantly reduced the efficiency of labeling from 95% to 6% (Fig. 2A), consistent with labeling of the deprotonated carboxylate group of E73.

3.2. E73 forms a specific binding site for neurosteroids and cholesterol

Singular labeling by 5α-6-AziP of the nucleophilic E73 side chain suggests the possibility that this is a non-specific phenomenon and that E73 does not form a specific neurosteroid binding site. We used three approaches to test this hypothesis.

First, we photolabeled the E73Q mutant of mVDAC1 with 5α-6-AziP (100 μM three times). An E73Q mutation removes the nucleophilic glutamate side chain, but is not likely to significantly perturb a putative sterol binding pocket. Intact protein MS analysis of the photolabeled sample showed a marked reduction in labeling efficiency (> 95% in WT to 5% in E73Q) (Fig. 2B). LC-MS/MS of tryptic digests of the photolabeled sample revealed two photolabeled peptides, which localize 5α-6-AziP labeling to both Y67 and Y62-R63 (Fig. 2C and D, Table 1). Y62, which faces the membrane is more likely to be the photolabeled residue than R63, which faces the hydrophilic pore. Both Y62 and Y67 are nucleophilic residues near E73 (Fig. 2E); Y62 was also photolabeled by a cholesterol labeling reagent in the E73Q mutant [11]. Thus, mutation of E73 to a glutamine results in labeling of two nucleophilic residues near position 73. Of the multiple tyrosine and glutamate residues in the transmembrane domain of mVDAC1, only those near E73 were labeled by 5α-6-AziP (Fig. 2F), consistent with the conclusion that neurosteroids bind to a site near E73.

In a second approach, we examined whether the addition of excess allopregnanolone or cholesterol competitively prevent 5α-6-AziP photolabeling of E73. WT mVDAC1 was photolabeled with 1 μM 5α-6-AziP in the absence or presence of 30 μM allopregnanolone or cholesterol. Photolabeling efficiencies were estimated from extracted ion chromatograms of unlabeled and photolabeled tryptic peptides as previously described [23]. Allopregnanolone and cholesterol significantly reduce 5α-6-AziP photolabeling of E73 (Fig. 3) indicating that both the neurosteroid, allopregnanolone and cholesterol bind specifically to this site.

In a third approach, we photolabeled WT mVDAC1 with the TPD-based reagent, KK200 (100 μM three times). Intact protein MS showed three peaks corresponding to unlabeled mVDAC1, mVDAC1 labeled with one KK200 (22% efficiency), and mVDAC1 labeled with two KK200 (3% efficiency) (Fig. 4A). Assuming that the probability of KK200 photolabeling any given site is independent of labeling other sites, the expected abundances of mVDAC1 species with one or more photolabels is the product of the individual probabilities of labeling each site. Since 5α-6-AziP labels mVDAC1 with 100% efficiency, and yet a doubly-labeled species is low abundance, this clearly demonstrates that 5α-6-AziP does not label sites other than E73 with significant efficiency. However, since KK200 labels mVDAC1 with only ~25% efficiency, the presence of a doubly-labeled species strongly suggests the presence of two or more labeled sites. Consistent with this, top-down fragmentation with HCD showed one *b* ion and two *y* ions that delineate two or more photolabeled residues at different regions of the protein (Fig. 4B). Multiple photolabeled residues were then identified by LC-MS/MS analysis of tryptic digests, which will be detailed below. Of these sites, one was of particular interest with regards to E73: KK200 photolabeled F99 (Fig. 4C, Table 1). F99 is near E73, separated by one β-strand (Fig. 4D). To examine the possibility that KK200 is photolabeling F99 from within a sterol pocket near E73, we docked KK200 to the mVDAC1 crystal structure in a 22 Å × 22 Å × 28 Å box centered at E73. This yielded multiple poses with the TPD photo-labeling moiety adjacent to F99 and the steroid backbone near E73. One such pose places the TPD diaziryl group 3.7 Å from the F99 side chain, the 3-hydroxyl 2.3 Å from the E73 carbonyl where it could form a hydrogen bond, and the 6-position (where the diazirine is located in 5α-6-AziP) 4 Å from E73 (Fig. 4D). This docking result shows that the dimensions of KK200 are compatible with photolabeling of F99 from within a binding site at E73.

Taken together, the photolabeling data define a sterol binding pocket formed by E73, Y62, and F99. T83, which is also located within this pocket, was previously photolabeled by the cholesterol reagent, LKM38 [11]. A surface representation of this region in mVDAC1 shows a groove extending from E73 and Y62 to F99 (Fig. 5). To explore sterol binding modes within this pocket, we docked allopregnanolone and cholesterol to a 16 Å × 16 Å × 13 Å box delimited by these photo-labeled residues. All docked poses were clustered with 2 Å RMSD. Within this site, two clusters of poses with similar binding energies were identified for both allopregnanolone (Fig. 5A) and cholesterol (Fig. 5B) with the sterol oriented in opposite directions along this groove (i.e. either the 3-position or 17-position is adjacent to E73). For poses where the 3-position is adjacent to E73, the 3α stereochemistry of allopregnanolone places its 3-hydroxyl ~1.9 Å from the E73 carbonyl, which would form a strong hydrogen bond (Fig. 5A, *left*). In contrast, in the same orientation, the 3β stereochemistry of cholesterol places its 3-hydroxyl ~5.4 Å from the E73 carbonyl (Fig. 5B, *left*).

In summary, there is a specific sterol binding pocket in mVDAC1, centered on E73, that can be occupied by either neurosteroids or cholesterol. While photolabeling reagents with aliphatic diazirines may diffuse some distance before labeling, TPD-based reagents are likely to label the protein pre*cis*ely at its binding location. The favorable photochemistry of KK200 maps a putative binding orientation for neurosteroids within this pocket where the 3-position is proximal to E73 and the 17-substituent to F99.

3.3. KK200 photolabels four additional sterol binding sites in mVDAC1

Four additional labeled peptides were identified for KK200 photolabeling of WT mVDAC1. HCD fragmentation spectra showed these labeled residues to be C127, G192, L245 and L279-E280 (Figs. 6A, C, 7A and C; Table 1). Since L279 is facing the membrane and E280 the pore, we favor KK200 labeling of L279. KK200 labeling of these hydrophobic amino acids is consistent with its photochemistry of carbenemediated labeling, and suggestive that labeling by the TPD group is occurring pre*cis*ely at the sterol binding site. Examination of these residues in the mVDAC1 crystal structure shows that they are adjacent to or within hydrophobic pockets previously proposed to be cholesterol binding sites by docking and MD simulations (Figs. 6B, D, 7B, D).

To examine whether these sites are also common neurosteroid and cholesterol binding sites, we photolabeled WT mVDAC1 with 10 μM KK200 in the absence or presence of 100 μM allopregnanolone or cholesterol. At 10 μM KK200, photolabeling of F99 and L279 was not detectable. Photolabeling of C127, G192, and L245 was detected at efficiencies of 5.3 ± 0.9%, 1.6 ± 0.2% and 1.3 ± 0.3%, respectively (± SD). Allopregnanolone and cholesterol both significantly reduced the efficiency of labeling, indicating that these sites are specific sterol binding sites (Fig. 8).

3.4. Allopregnanolone does not alter voltage-dependent gating of mVDAC1

Specific binding of neurosteroids or cholesterol at multiple sites in mVDAC1 raises the possibility that sterols modulate mVDAC1 ion transport function. Sterols have been reported to activate VDAC1 function from rat liver [17], although we recently reported that cholesterol does not alter voltage-dependent gating of mVDAC1 reconstituted in lipid bilayers [18]. To test whether neurosteroids affect voltage-dependent gating of mVDAC1, multi-channel currents were measured of mVDAC1 in lipid bilayers before and after addition of 3, 10 and 30 μM allopregnanolone to both sides of the membrane in response to an applied triangular voltage wave [18,31]. Allopregnanolone addition up to 30 μM did not affect mVDAC1 normalized conductance (Fig. 9A) and probability to be open (P_{open}, Fig. 9B). The gating parameters—the effective gating charge, n, and the voltage at which half of the channels are open, V_0—were obtained from fitting of P_{open} vs. V plot with the Boltzmann equation (solid lines in Fig. 9B), and are shown in Fig. 9C. There is no significant effect of allopregnanolone addition on mVDAC1 gating parameters. To test allopregnanolone partitioning into the lipid bilayer, we performed independent experiments using a channel-forming polypeptide, gramicidin A, which is a highly sensitive molecular probe of lipid bilayer mechanics [10,32,33]. Several studies have demonstrated that the lifetime of a gramicidin A conducting dimer is exquisitely sensitive to partitioning of hydrophobic compounds into the membrane due to changes in bilayer thickeness, lipid packing stress or bilayer curvature [32,33]. Application of allopregnanolone, as performed in the mVDAC1 experiments, resulted in a dose-dependent increase in the lifetime of gramicidin currents, indicating that allopregnanolone partitions in the planar lipid bilayer (Supplementary Fig. S1), yet has no significant effect on mVDAC1 gating properties.

4. Discussion

The β-barrel outer mitochondrial membrane porin, VDAC1, is regulated by a diverse number of ligands and proteins [1,34,35], and its roles in mitochondrial metabolism and apoptosis make it a potential therapeutic target in cancer and neurodegenerative disorders [9,36]. Proteome-wide photolabeling using neurosteroid or cholesterol re-agents in rat brain [16] or mammalian cell lines [15] have found VDAC1 to be one of the most efficiently photolabeled targets. This is due to singular labeling of E73. The unique position of E73 in the transmembrane region raises the concern that this labeling is due to non-specific targeting of a nucleophilic residue. We present multiple lines of evidence that argue for a specific site at E73. We define specific binding as binding to a saturable site [37]. Based on this definition, competitive prevention of labeling at E73 by both allopregnanolone and cholesterol demonstrates saturable occupancy of the photolabeled site by these sterols, and confirms specific binding.

In addition to saturable binding, the E73 site is also targeted by another photolabeling reagent, KK200, which labeled F99. Remarkably, docking KK200 to this site, such that the TPD group is adjacent to F99, places the steroid 3-hydroxyl 2.3 Å and the 6-position (where the diazirine is located) 4 Å from the E73 carbonyl. Docked poses of allopregnanolone in this orientation also show the 3-hydroxyl ~2 Å from E73. We speculate that this represents a preferred binding orientation for 3α,5α-neurosteroids at this site that may be driven by a hydrogen bond interaction between the 3-hydroxyl and E73 carbonyl (Fig. 5A, *left*), as has been reported in the GABA(A) receptor [38]. Consistent with this, our photolabeling data with 3α,5α-neurosteroids (5α-6-AziP and KK200) place the 6-position close to E73 and 17-position close to F99. In contrast, docked poses of cholesterol do not show the presence of a hydrogen bond between its 3-hydroxyl and E73 because of the β-stereochemistry of the 3-hydroxyl group (Fig. 5B, *left*). Without this hydrogen bond, cholesterol may bind preferably in the opposite orientation with the aliphatic tail adjacent to E73 (Fig. 5B, *right*). Consistent with this, cholesterol analogues photolabel this site such that the 7-position (LKM38) labels T83 and the aliphatic tail (KK174) labels E73 [11]. Taken together, photolabeling of mVDAC1 reconstituted in bicelles has delineated a specific binding site at E73 that is common to neurosteroids and cholesterol. In addition to saturable sterol binding at this site, identification of multiple photolabeled residues by different reagents map distinct points within this pocket, and further substantiate the specificity of this sterol binding site. Interestingly, these photo-labeled residues suggest that 3α,5α-neurosteroids and cholesterol preferentially fit in this binding groove in opposite orientations.

E73 has been implicated in multiple aspects of VDAC1 function including mVDAC1 dimerization [21], hexokinase-mediated apoptosis [20], and coordination of calcium [4]. VDAC protein dynamics are also significantly determined by the charge of E73 [39]. Recently, it was shown that mutations of E73, or the addition of cholesterol [18] do not affect voltage-dependent gating of mVDAC1. Here, we show that allopregnanolone also does not affect mVDAC1 voltage-dependent gating. However, sterol binding to E73 may affect other modes of modulation such as oligomerization, and binding of hexokinase or other mitochondrial outer membrane proteins such as 18 kDa Translocator Protein, TSPO [40]. Indeed, protonation of E73 has been shown to determine dimerization of mVDAC1

[21], and it is conceivable that protonation of E73 and VDAC1 dimerization may occlude sterol binding or that sterol binding may modulate VDAC1 dimerization. While the physiologic significance of VDAC dimerization is unknown, we speculate that it is unlikely to alter ion transport, but may influence VDAC complex formation with other mitochondrial protein such as the Bcl2-family proteins. Interestingly, it was recently shown that ceramides induce apoptosis by binding to VDAC2 at a site near E84, the equivalent residue to E73 in VDAC1 [41]. Given the low abundance of cholesterol and neurosteroids in mitochondria [42], it is possible that these sites are occupied by other endogenous lipids such as phospholipids or ceramides under most physiologic conditions. However, this may be altered under conditions where mitochondrial sterol content increase. For example, increased mitochondrial cholesterol levels are associated with certain pathologic conditions such as chemotherapy resistance in cancer [43]. In addition, the cholesterol analogue, Olesoxime, has been found to have neuroprotective effects by targeting mitochondria [44], and neurosteroids are neuroprotective in conditions such as traumatic or ischemic brain injury [45,46], possibly by acting on mitochondria [47–49]. Our work raises the hypothesis that sterols such as neurosteroids also bind to the equivalent E84 site in VDAC2, and that antagonism of ceramides at this site mediates their anti-apoptotic effect.

Four additional sterol binding sites were identified by photolabeling with KK200. These photolabeled residues match with sites previously proposed by docking and MD simulations [14]. The sites determined by modeling were designated 1 through 5 [14]. These sites correspond with our photolabeled residues as follows: C127 with site 1, G192 sites 2 and 3, L245 site 4, and L279 site 5. Thus, we have identified E73 as well as these four sites for a total of five sterol binding sites consistent with biochemical evidence that VDAC1 co-purifies with five cholesterol molecules per protein [19]. When comparing the murine and human VDAC1 sequences, which have 98.6% identity, all five photolabeled sites are conserved, indicating that these sites are likely to also be present in the human VDAC1 protein. Furthermore, our competition experiments suggest that at least four of these sites (i.e. E73/F99, C127, G192, L245) can be occupied by both neurosteroids and cholesterol, a finding that was also recently demonstrated in the pentameric ligand-gated ion channel, GLIC [50]. We suspect that this phenomenon is prevalent among membrane proteins, and suggests regulatory mechanisms whereby different sterols compete for common sites to exert different modulatory effects. For example, our photolabeling data suggest that 3α,5α-neurosteroids and cholesterol bind to the E73 site in opposite orientations, which would result in different contact points within the binding pocket and potentially, different effects on mVDAC1 function. Given the relative promiscuity of these sites for allopregnanolone, cholesterol and other lipids such as ceramide [41], it is interesting to speculate that other steroids may bind to VDAC1 within the mitochondria, which is a center for the synthesis of many steroids including oxysterols, bile acids and steroid hormones [51].

In conclusion, mVDAC1 has five sterol binding sites, at least three of which are shared by the neurosteroid, allopregnanolone, and cholesterol. Importantly, our data presents convincing evidence that E73 forms a specific sterol binding site, in which neurosteroids and cholesterol may bind with different orientations. While neurosteroid binding to mVDAC1 does not alter voltage-dependent gating of this channel, the structural and functional importance of E73 suggest the possibility that sterols may modulate other aspects of VDAC1

function such as channel dimerization or hexokinase-mediated signaling, by binding to shared, specific sites.

Supplementary Material

Refer to Web version on PubMed Central for supplementary material.

Acknowledgements

M.Q.-M. and T.K.R. are indebted to Sergey Bezrukov (NICHD, NIH) for fruitful discussions.

Funding

This work was supported by the National Institutes of Health K08GM126336, R01GM108799, R01GM078844, P01GM47969, and an intramural research program (NICHD); the National Science Foundation DGE-1143954, and the Taylor Family Institute for Innovative Psychiatric Research.

References

[1]. McCommis KS, Baines CP, The role of VDAC in cell death: friend or foe? Biochim. Biophys. Acta 1818 (2012) 1444–1450. [PubMed: 22062421]

[2]. Colombini M, Voltage gating in the mitochondrial channel, VDAC, J. Membr. Biol 111 (1989) 103–111. [PubMed: 2482359]

[3]. Bathori G, Csordas G, Garcia-Perez C, Davies E, Hajnoczky G, Ca2+-dependent control of the permeability properties of the mitochondrial outer membrane and voltage-dependent anion-selective channel (VDAC), J. Biol. Chem 281 (2006) 17347–17358. [PubMed: 16597621]

[4]. Israelson A, Abu-Hamad S, Zaid H, Nahon E, Shoshan-Barmatz V, Localization of the voltage-dependent anion channel-1 Ca2+-binding sites, Cell Calcium 41 (2007) 235–244. [PubMed: 16930689]

[5]. Azoulay-Zohar H, Israelson A, Abu-Hamad S, Shoshan-Barmatz V, In self-defence: hexokinase promotes voltage-dependent anion channel closure and prevents mitochondria-mediated apoptotic cell death, Biochem. J 377 (2004) 347–355. [PubMed: 14561215]

[6]. Arzoine L, Zilberberg N, Ben-Romano R, Shoshan-Barmatz V, Voltage-dependent anion channel 1-based peptides interact with hexokinase to prevent its anti-apoptotic activity, J. Biol. Chem 284 (2009) 3946–3955. [PubMed: 19049977]

[7]. Rostovtseva TK, Sheldon KL, Hassanzadeh E, Monge C, Saks V, Bezrukov SM, Sackett DL, Tubulin binding blocks mitochondrial voltage-dependent anion channel and regulates respiration, Proc. Natl. Acad. Sci. U. S. A 105 (2008) 18746–18751. [PubMed: 19033201]

[8]. Rostovtseva TK, Gurnev PA, Protchenko O, Hoogerheide DP, Yap TL, Philpott CC, Lee JC, Bezrukov SM, alpha-Synuclein shows high affinity interaction with voltage-dependent anion channel, suggesting mechanisms of mitochondrial regulation and toxicity in Parkinson disease, J. Biol. Chem 290 (2015) 18467–18477. [PubMed: 26055708]

[9]. Shoshan-Barmatz V, Ben-Hail D, VDAC, a multi-functional mitochondrial protein as a pharmacological target, Mitochondrion 12 (2012) 24–34. [PubMed: 21530686]

[10]. Rostovtseva TK, Kazemi N, Weinrich M, Bezrukov SM, Voltage gating of VDAC is regulated by nonlamellar lipids of mitochondrial membranes, J. Biol. Chem 281 (2006) 37496–37506. [PubMed: 16990283]

[11]. Budelier MM, Cheng WWL, Bergdoll L, Chen ZW, Janetka JW, Abramson J, Krishnan K, Mydock-McGrane L, Covey DF, Whitelegge JP, Evers AS, Photoaffinity labeling with cholesterol analogues precisely maps a cholesterol-binding site in voltage-dependent anion channel-1, J. Biol. Chem 292 (2017) 9294–9304. [PubMed: 28396346]

[12]. Budelier MM, Cheng WW, Bergdoll L, Chen ZW, Abramson J, Krishnan K, Qian M, Covey DF, Janetka JW, Evers AS, Click chemistry reagent for identification of sites of covalent ligand

incorporation in integral membrane proteins, Anal. Chem 89 (2017) 2636–2644. [PubMed: 28194953]

[13]. Hiller S, Garces RG, Malia TJ, Orekhov VY, Colombini M, Wagner G, Solution structure of the integral human membrane protein VDAC-1 in detergent micelles, Science 321 (2008) 1206–1210. [PubMed: 18755977]

[14]. Weiser BP, Salari R, Eckenhoff RG, Brannigan G, Computational investigation of cholesterol binding sites on mitochondrial VDAC, J. Phys. Chem. B 118 (2014) 9852–9860. [PubMed: 25080204]

[15]. Hulce JJ, Cognetta AB, Niphakis MJ, Tully SE, Cravatt BF, Proteome-wide mapping of cholesterol-interacting proteins in mammalian cells, Nat. Methods 10 (2013) 259–264. [PubMed: 23396283]

[16]. Darbandi-Tonkabon R, Hastings WR, Zeng CM, Akk G, Manion BD, Bracamontes JR, Steinbach JH, Mennerick SJ, Covey DF, Evers AS, Photoaffinity labeling with a neuroactive steroid analogue. 6-azi-pregnanolone labels voltage-dependent anion channel-1 in rat brain, J. Biol. Chem 278 (2003) 13196–13206. [PubMed: 12560326]

[17]. Popp B, Schmid A, Benz R, Role of sterols in the functional reconstitution of water-soluble mitochondrial porins from different organisms, Biochemistry 34 (1995) 3352–3361. [PubMed: 7533536]

[18]. Queralt-Martin M, Bergdoll L, Jacobs D, Bezrukov SM, Abramson J, Rostovtseva TK, Assessing the role of residue E73 and lipid headgroup charge in VDAC1 voltage gating, Biochim. Biophys. Acta Bioenerg 1860 (2019) 22–29. [PubMed: 30412693]

[19]. De Pinto V, Benz R, Palmieri F, Interaction of non-classical detergents with the mitochondrial porin. A new purification procedure and characterization of the pore-forming unit, European journal of biochemistry/FEBS 183 (1989) 179–187.

[20]. Zaid H, Abu-Hamad S, Israelson A, Nathan I, Shoshan-Barmatz V, The voltage-dependent anion channel-1 modulates apoptotic cell death, Cell Death Differ 12 (2005) 751–760. [PubMed: 15818409]

[21]. Bergdoll LA, Lerch MT, Patrick JW, Belardo K, Altenbach C, Bisignano P, Laganowsky A, Grabe M, Hubbell WL, Abramson J, Protonation state of glutamate 73 regulates the formation of a specific dimeric association of mVDAC1, Proc. Natl. Acad. Sci. U. S. A 115 (2018) E172–E179. [PubMed: 29279396]

[22]. Ujwal R, Cascio D, Colletier JP, Faham S, Zhang J, Toro L, Ping P, Abramson J, The crystal structure of mouse VDAC1 at 2.3 A resolution reveals mechanistic insights into metabolite gating, Proc. Natl. Acad. Sci. U. S. A 105 (2008) 17742–17747. [PubMed: 18988731]

[23]. Cheng WWL, Chen ZW, Bracamontes JR, Budelier MM, Krishnan K, Shin DJ, Wang C, Jiang X, Covey DF, Akk G, Evers AS, Mapping two neurosteroid-modulatory sites in the prototypic pentameric ligand-gated ion channel GLIC, J. Biol. Chem 293 (2018) 3013–3027. [PubMed: 29301936]

[24]. Wessel D, Flugge UI, A method for the quantitative recovery of protein in dilute solution in the presence of detergents and lipids, Anal. Biochem 138 (1984) 141–143. [PubMed: 6731838]

[25]. Zhang Z, Marshall AG, A universal algorithm for fast and automated charge state deconvolution of electrospray mass-to-charge ratio spectra, J. Am. Soc. Mass Spectrom 9 (1998) 225–233. [PubMed: 9879360]

[26]. Guner H, Close PL, Cai W, Zhang H, Peng Y, Gregorich ZR, Ge Y, MASH Suite: a user-friendly and versatile software interface for high-resolution mass spectrometry data interpretation and visualization, J. Am. Soc. Mass Spectrom 25 (2014) 464–470. [PubMed: 24385400]

[27]. Morris GM, Huey R, Lindstrom W, Sanner MF, Belew RK, Goodsell DS, Olson AJ, AutoDock4 and AutoDockTools4: automated docking with selective receptor flexibility, J. Comput. Chem 30 (2009) 2785–2791. [PubMed: 19399780]

[28]. Rappaport SM, Teijido O, Hoogerheide DP, Rostovtseva TK, Berezhkovskii AM, Bezrukov SM, Conductance hysteresis in the voltage-dependent anion channel, Eur. Biophys. J 44 (2015) 465–472. [PubMed: 26094068]

[29]. Faham S, Bowie JU, Bicelle crystallization: a new method for crystallizing membrane proteins yields a monomeric bacteriorhodopsin structure, J. Mol. Biol 316 (2002) 1–6. [PubMed: 11829498]

[30]. Chen ZW, Bracamontes JR, Budelier MM, Germann AL, Shin DJ, Kathiresan K, Qian MX, Manion B, Cheng WWL, Reichert DE, Akk G, Covey DF, Evers AS, Multiple functional neurosteroid binding sites on GABAA receptors, PLoS Biol 17 (2019) e3000157. [PubMed: 30845142]

[31]. Teijido O, Rappaport SM, Chamberlin A, Noskov SY, Aguilella VM, Rostovtseva TK, Bezrukov SM, Acidification asymmetrically affects voltage-dependent anion channel implicating the involvement of salt bridges, J. Biol. Chem 289 (2014) 23670–23682. [PubMed: 24962576]

[32]. Lundbaek JA, Collingwood SA, Ingolfsson HI, Kapoor R, Andersen OS, Lipid bilayer regulation of membrane protein function: gramicidin channels as molecular force probes, J. R. Soc. Interface 7 (2010) 373–395. [PubMed: 19940001]

[33]. Rusinova R, Koeppe RE 2nd, O.S. Andersen, A general mechanism for drug promiscuity: studies with amiodarone and other antiarrhythmics, J Gen Physiol 146 (2015) 463–475. [PubMed: 26573624]

[34]. Arbel N, Shoshan-Barmatz V, Voltage-dependent anion channel 1-based peptides interact with Bcl-2 to prevent antiapoptotic activity, J. Biol. Chem 285 (2010) 6053–6062. [PubMed: 20037155]

[35]. Reina S, De Pinto V, Anti-cancer compounds targeted to VDAC: potential and perspectives, Curr. Med. Chem 24 (2017) 4447–4469. [PubMed: 28554318]

[36]. Magri A, Messina A, Interactions of VDAC with proteins involved in neurode-generative aggregation: an opportunity for advancement on therapeutic molecules, Curr. Med. Chem 24 (2017) 4470–4487. [PubMed: 28571556]

[37]. Maguire JJ, Kuc RE, Davenport AP, Radioligand binding assays and their analysis, Methods Mol. Biol 897 (2012) 31–77. [PubMed: 22674160]

[38]. Chen ZWB J. R.; Budelier MM; Germann AL; Shin DJ; Kathiresan K; Qian MX; Manion B; Cheng WWL; Reichert DE; Akk G; Covey DF; Evers AS, Identification of Multiple Functional Neurosteroid Binding Sites on GABAA Receptors, PLoS Biol, Press, 2019.

[39]. Villinger S, Briones R, Giller K, Zachariae U, Lange A, de Groot BL, Griesinger C, Becker S, Zweckstetter M, Functional dynamics in the voltage-dependent anion channel, Proc. Natl. Acad. Sci. U. S. A 107 (2010) 22546–22551. [PubMed: 21148773]

[40]. Gatliff J, East D, Crosby J, Abeti R, Harvey R, Craigen W, Parker P, Campanella M, TSPO interacts with VDAC1 and triggers a ROS-mediated inhibition of mitochondrial quality control, Autophagy 10 (2014) 2279–2296. [PubMed: 25470454]

[41]. Dadsena S, Bockelmann S, Mina JGM, Hassan DG, Korneev S, Razzera G, Jahn H, Niekamp P, Muller D, Schneider M, Tafesse FG, Marrink SJ, Melo MN, Holthuis JCM, Ceramides bind VDAC2 to trigger mitochondrial apoptosis, Nat. Commun 10 (2019) 1832. [PubMed: 31015432]

[42]. Horvath SE, Daum G, Lipids of mitochondria, Prog. Lipid Res 52 (2013) 590–614. [PubMed: 24007978]

[43]. Montero J, Morales A, Llacuna L, Lluis JM, Terrones O, Basanez G, Antonsson B, Prieto J, Garcia-Ruiz C, Colell A, Fernandez-Checa JC, Mitochondrial cholesterol contributes to chemotherapy resistance in hepatocellular carcinoma, Cancer Res 68 (2008) 5246–5256. [PubMed: 18593925]

[44]. Bordet T, Berna P, Abitbol JL, Pruss RM, Olesoxime (TRO19622): a novel mitochondrial-targeted neuroprotective compound, Pharmaceuticals (Basel) 3 (2010) 345–368. [PubMed: 27713255]

[45]. Djebaili M, Hoffman SW, Stein DG, Allopregnanolone and progesterone decrease cell death and cognitive deficits after a contusion of the rat pre-frontal cortex, Neuroscience 123 (2004) 349–359. [PubMed: 14698743]

[46]. Sayeed I, Guo Q, Hoffman SW, Stein DG, Allopregnanolone, a progesterone metabolite, is more effective than progesterone in reducing cortical infarct volume after transient middle cerebral artery occlusion, Ann. Emerg. Med 47 (2006) 381–389. [PubMed: 16546625]

[47]. Kaasik A, Kalda A, Jaako K, Zharkovsky A, Dehydroepiandrosterone sulphate prevents oxygen-glucose deprivation-induced injury in cerebellar granule cell culture, Neuroscience 102 (2001) 427–432. [PubMed: 11166128]

[48]. Kaasik A, Safiulina D, Kalda A, Zharkovsky A, Dehydroepiandrosterone with other neurosteroids preserve neuronal mitochondria from calcium overload, J. Steroid Biochem. Mol. Biol 87 (2003) 97–103. [PubMed: 14630095]

[49]. Sayeed I, Parvez S, Wali B, Siemen D, Stein DG, Direct inhibition of the mitochondrial permeability transition pore: a possible mechanism for better neuroprotective effects of allopregnanolone over progesterone, Brain Res 1263 (2009) 165–173. [PubMed: 19368823]

[50]. Budelier MM, Cheng WWL, Chen ZW, Bracamontes JR, Sugasawa Y, Krishnan K, Mydock-McGrane L, Covey DF, Evers AS, Common binding sites for cholesterol and neurosteroids on a pentameric ligand-gated ion channel, Biochim. Biophys. Acta Mol. Cell Biol. Lipids 1864 (2018) 128–136. [PubMed: 30471426]

[51]. Miller WL, Steroid hormone synthesis in mitochondria, Mol. Cell. Endocrinol 379 (2013) 62–73. [PubMed: 23628605]

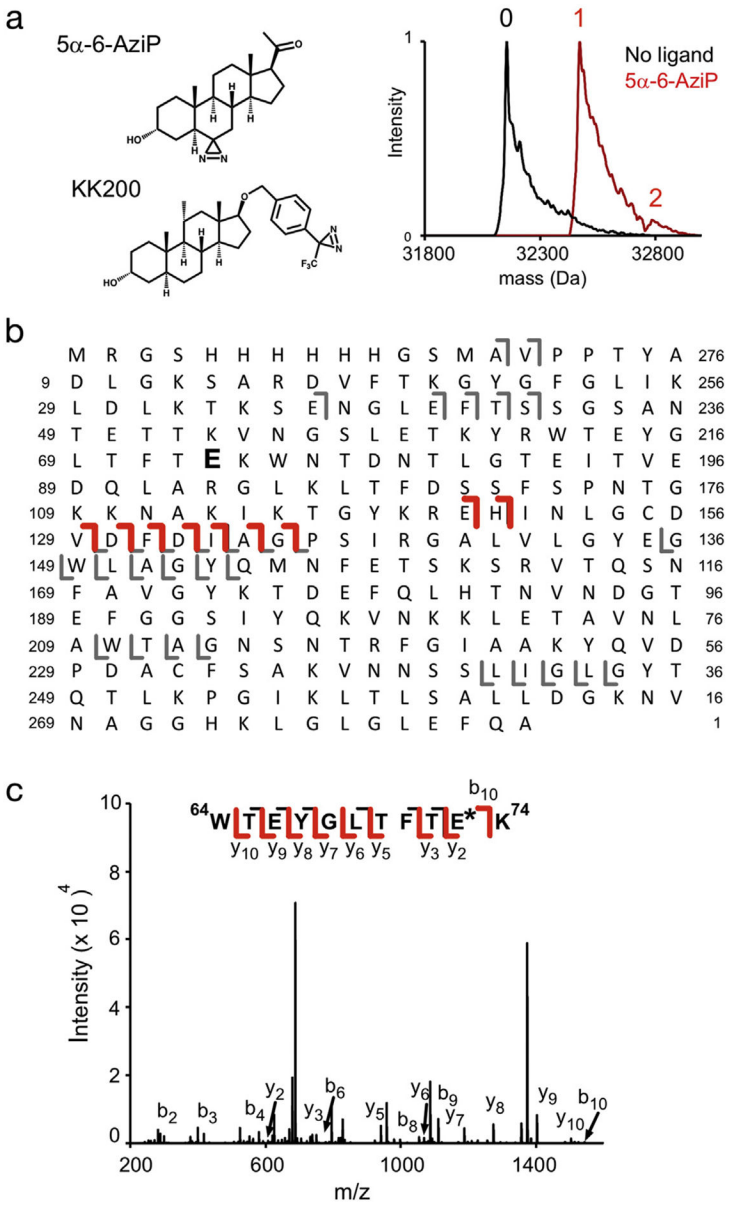

Fig. 1.

5α-6-AziP photolabels WT mVDAC1 with a stoichiometry of one at E73. (A) Left - Chemical structures of the allopregnanolone-based photolabeling reagents, 5α-6-AziP and KK200. Right - Deconvoluted spectra of WT mVDAC1 unlabeled (black, designated 0) and photolabeled with 5α-6-AziP 100 μM three times (red). The spectra of photolabeled mVDAC1 show a singly-labeled species (designated 1) with a tiny doubly-labeled species (designated 2) and no non-photolabeled species. (B) Fragment ion assignments for HCD of WT mVDAC1 photolabeled with one 5α-6-AziP. E73 is bolded; the numbering system shown in the figure is shifted by 12 residues due to the N-terminal His tag. Red and gray represents b and y ion fragments that do and do not contain the 5α-6-AziP modification, respectively. (C) Fragmentation (CID) spectrum of the indicated tryptic peptide from WT

mVDAC1 photolabeled with 5α-6-AziP at E73. Fragment ions containing 5α-6-AziP are shown in red.

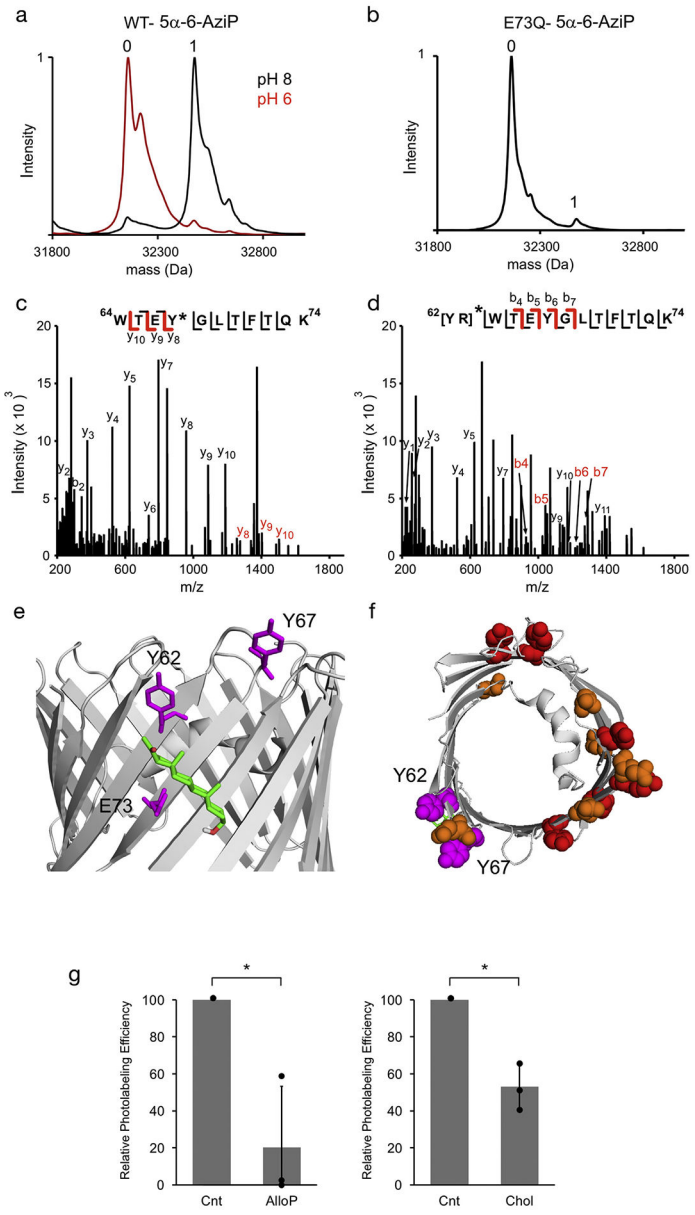

Fig. 2.

5α-6-AziP photolabels E73Q mVDAC1 at Y62 and Y67. (A) Deconvoluted spectra of WT mVDAC1 photolabeled with 5α-6-AziP 100 μM three times at pH 8 and pH 6. (B) Deconvoluted spectrum of E73Q mVDAC1 photolabeled with 5α-6-AziP 100 μM three times. (C) and (D) Fragmentation (HCD) spectra of the indicated tryptic peptides from E73Q mVDAC1 photolabeled with 5α-6-AziP at Y67 (C) and Y62-R63 (D). Fragment ions containing 5α-6-AziP are shown in red. (E) Crystal structure of mVDAC1 highlighting the photolabeled residues, E73, Y62, and Y67 (magenta), and showing the most prevalent docking pose of allopregnanolone (green) in the E73 site. (F) mVDAC1 structure viewed from top-down showing Y62 and Y67 side chains (magenta), and all other tyrosine (red) and glutamate (orange) residues with side chains facing the membrane.

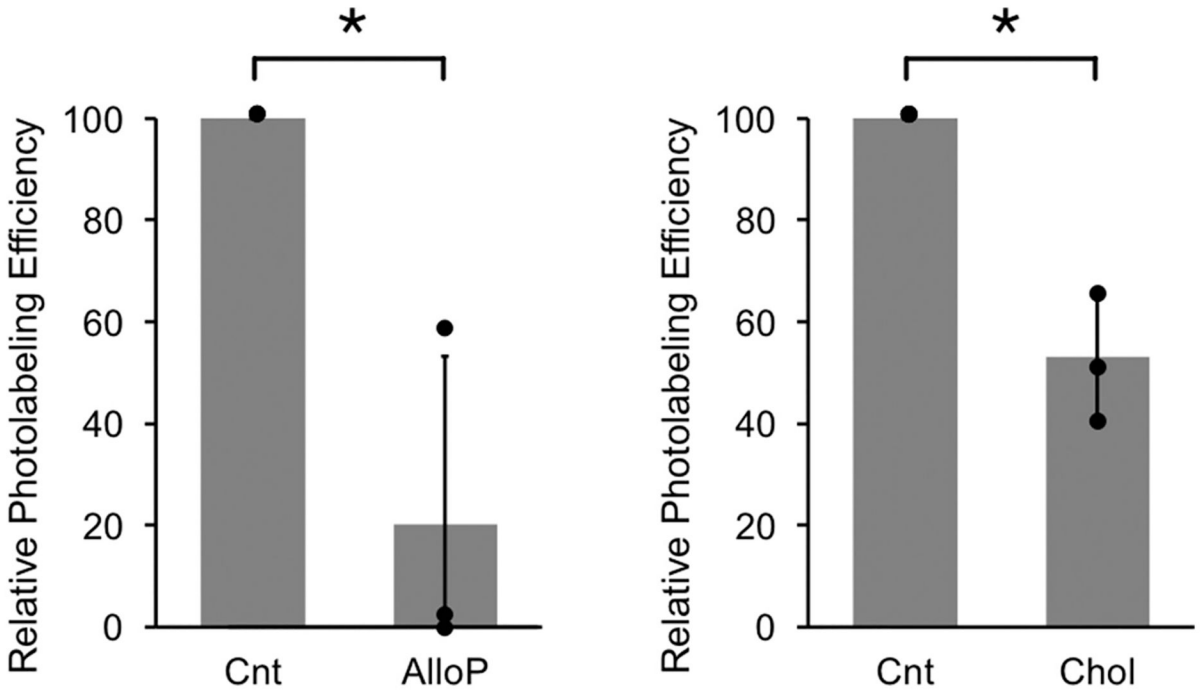

Fig. 3.

Allopregnanolone and cholesterol inhibit 5α-6-AziP photolabeling of E73. Relative photolabeling efficiencies of 1 μM 5α-6-AziP at E73 in the absence (Control- Cnt), or presence of 30 μM allopregnanolone (AlloP, *left*) or cholesterol (Chol, *right*). Photolabeling efficiencies were normalized to control in each replicate and then averaged (n = 3, ± SD, * indicates $p < 0.05$).

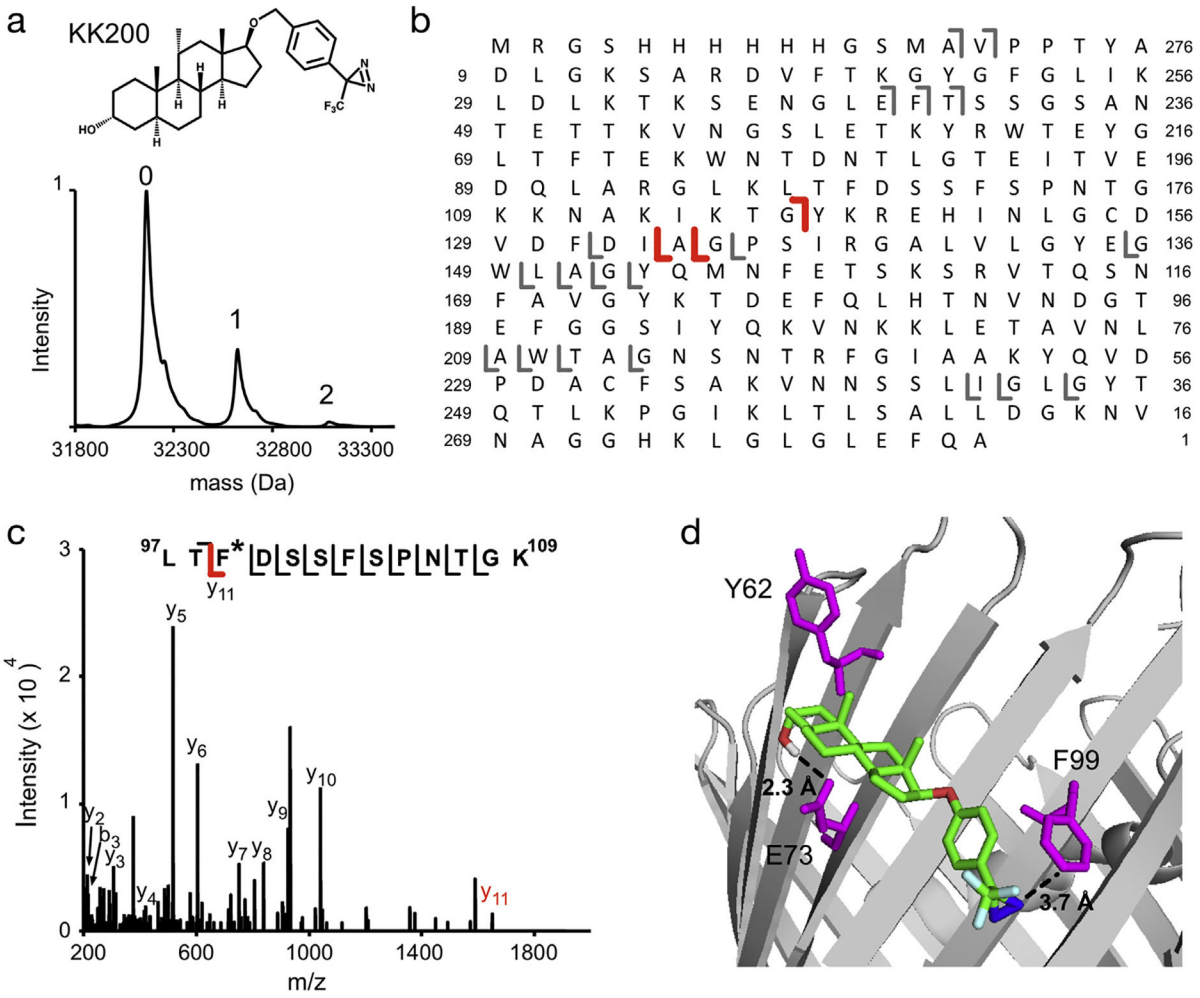

Fig. 4.

KK200 photolabels multiple sites in WT mVDAC1 including F99. (A) Deconvoluted spectra of WT mVDAC1 photolabeled with KK200 100 μM three times, showing an unlabeled species and a singly- and doubly-labeled species. (B) Fragment ion assignments for HCD of WT mVDAC1 photolabeled with one KK200. Red and gray represents *b* and *y* ion fragments that do and do not contain the KK200 modification, respectively. These ions indicate the presence of a KK200 modification N-terminal to G117 and C-terminal to G135. (C) Fragmentation (HCD) spectrum of the indicated tryptic peptide from WT mVDAC1 photo-labeled with KK200 at F99. The fragment ion y11 contains KK200 and is shown in red. (D) Crystal structure of mVDAC1 highlighting the photolabeled residues, E73 and F99 (magenta), and showing a representative pose of KK200 from one cluster of docked poses that places the TPD diazirine closest to F99.

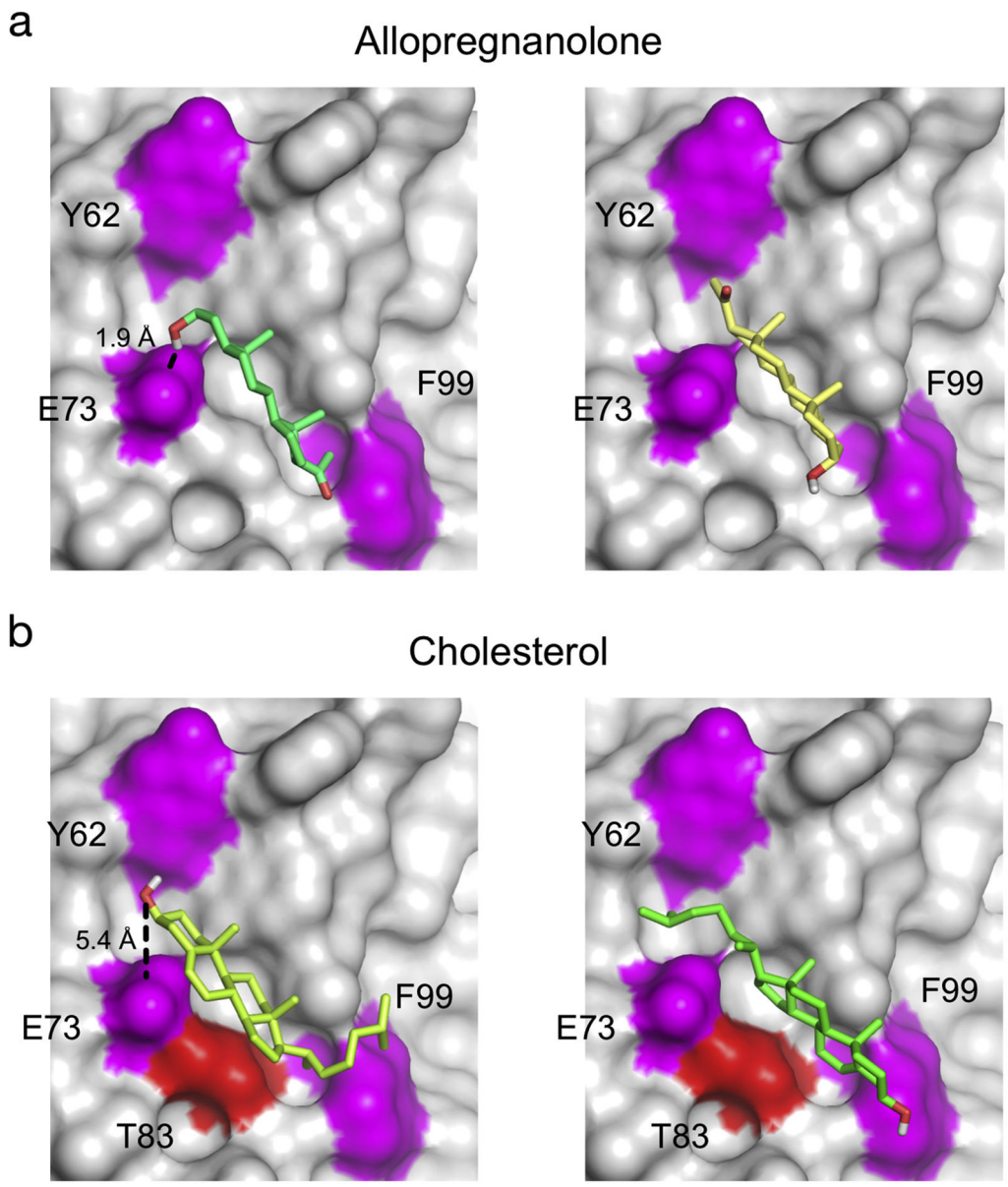

Fig. 5.

Allopregnanolone and Cholesterol Binding Modes in the E73 Site. (A) Structures of the two predominant clusters of docking poses for allopregnanolone within the binding groove formed by the photolabeled residues, E73, F99 and Y62 (magenta). mVDAC1 protein is shown as a surface representation. The pose on the left shows the 3-hydroxyl of allopregnanolone 1.9 Å from the E73 carbonyl. (B) Same as (A) for cholesterol highlighting the photolabeled residues, E73, F99 and Y62 (magenta) as well as T83 (red), photolabeled by the cholesterol analogue LKM38 [11]. The pose on the left shows the 3-hydroxyl of cholesterol 5.4 Å from the E73 carbonyl.

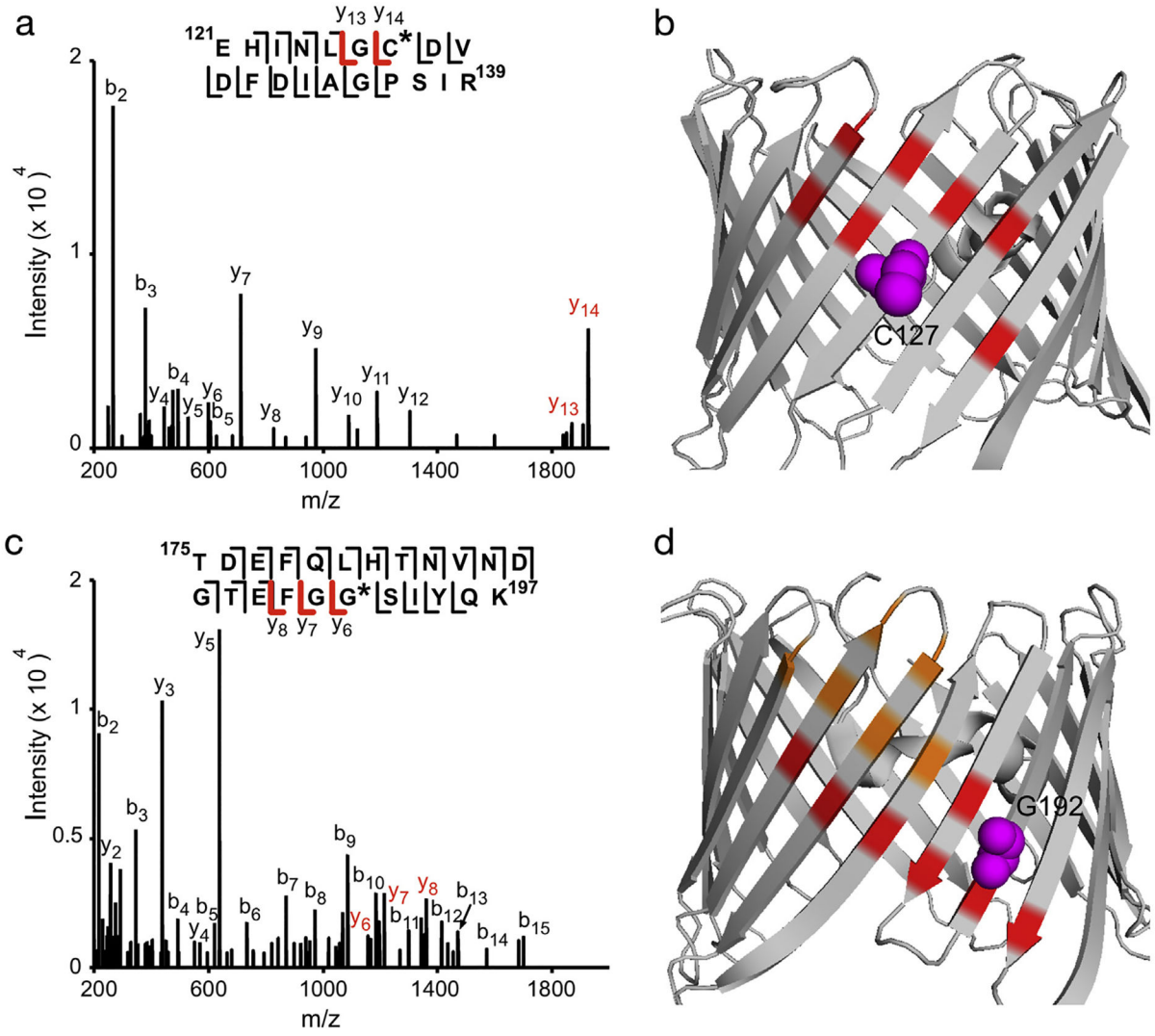

Fig. 6.

KK200 photolabels C127 and G192 in WT mVDAC1. (A) Fragmentation (HCD) spectrum of the indicated tryptic peptide from WT mVDAC1 photolabeled with KK200 at C127. Fragment ions containing KK200 are shown in red. (B) Crystal structure of mVDAC1 highlighting the photo-labeled residue, C127 (magenta), and residues from site 1 (red) [14]. (C) Same as (A) for another tryptic peptide photolabeled with KK200 at G192. (D) Same as (B) showing G192 (magenta) and sites 2 (orange) and 3 (red).

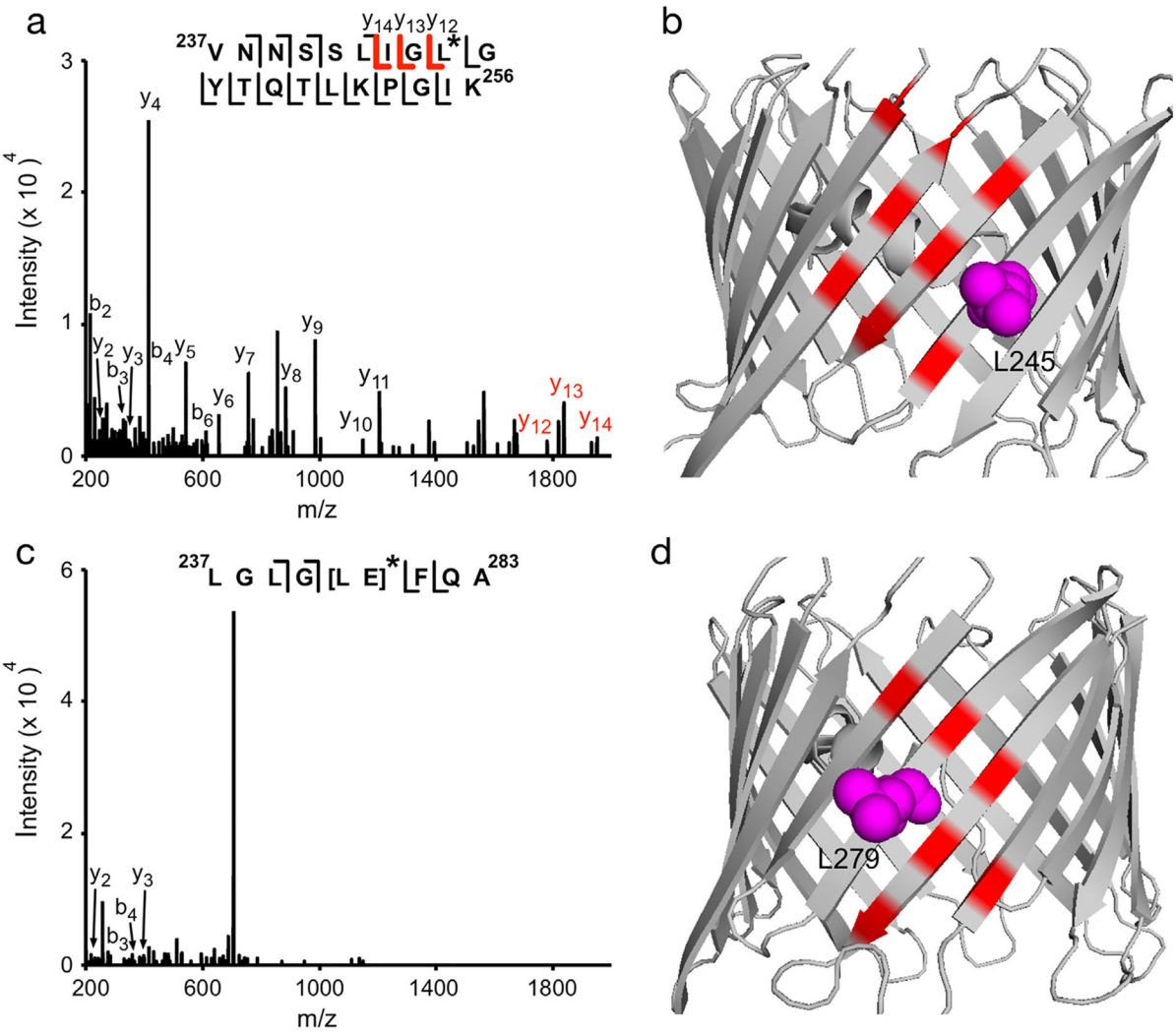

Fig. 7.

KK200 photolabels L245 and L279 in WT mVDAC1. (A) Fragmentation (HCD) spectrum of the indicated tryptic peptide from WT mVDAC1 photolabeled with KK200 at L245. Fragment ions containing KK200 are shown in red. (B) Crystal structure of mVDAC1 highlighting the photo-labeled residue, L245 (magenta), and residues from site 4 (red) [14]. (C) Same as (A) for another tryptic peptide photolabeled with KK200 at L279-E280. (D) Same as (B) showing L279 (magenta) and site 5 (red).

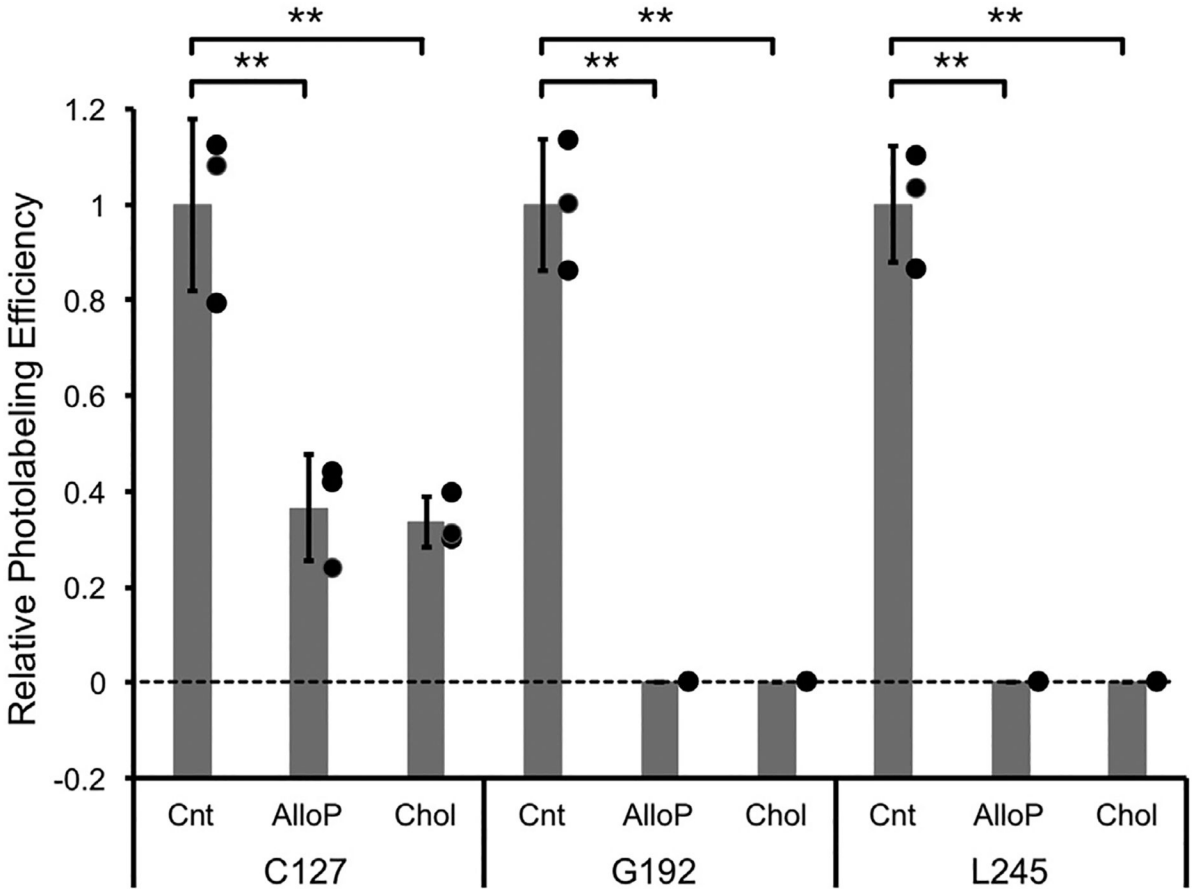

Fig. 8.

Allopregnanolone and cholesterol inhibit KK200 photolabeling. Relative photolabeling efficiency of 10 μM KK200 at C127, G192 and L245 in the absence (Control - Cnt), or presence of 100 μM allopregnanolone (AlloP) or cholesterol (Chol). Photolabeling efficiencies were normalized to the average of control (n = 3, ± SD, ** indicates $p < 0.01$).

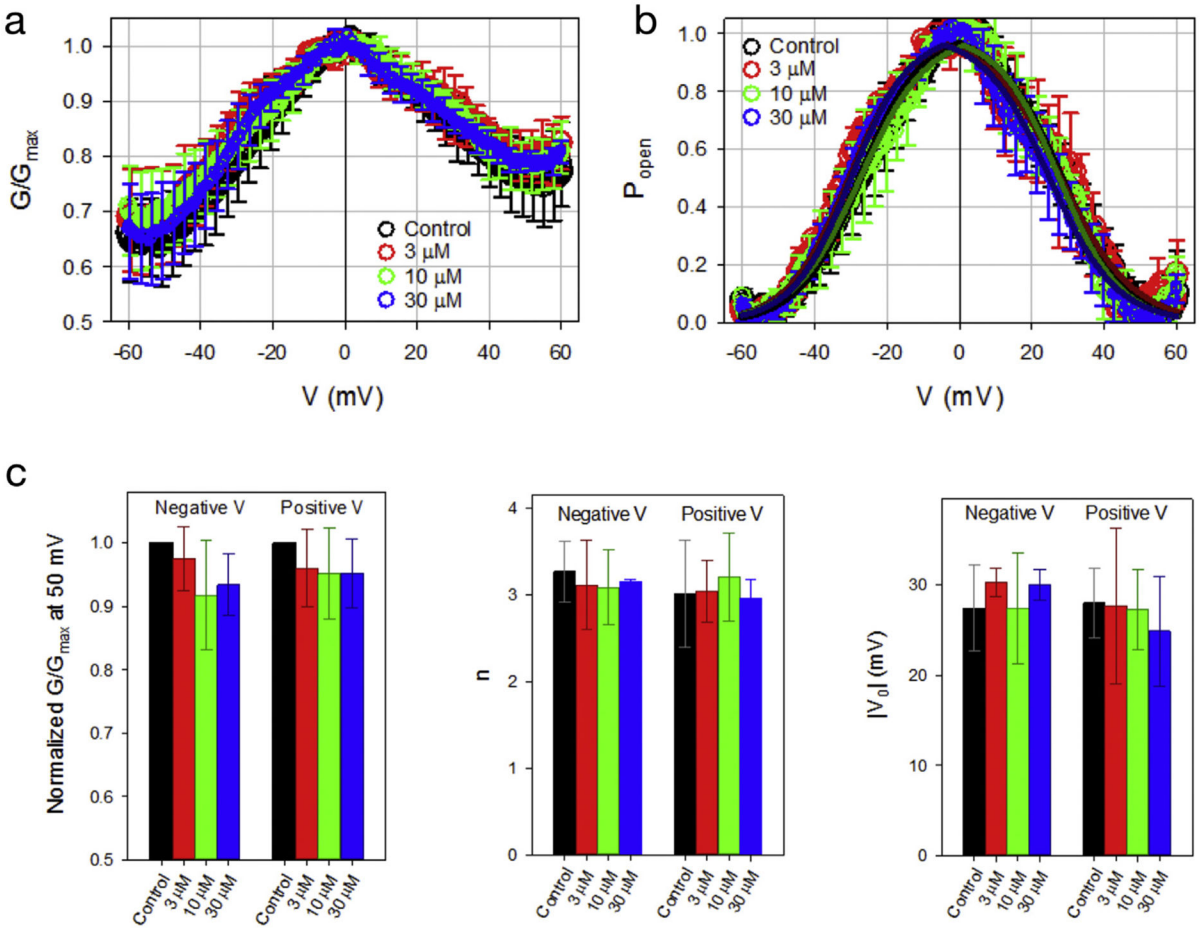

Fig. 9.

Allopregnanolone does not affect voltage-dependent gating of mVDAC1. (A) and (B) Plot of the normalized mVDAC1 conductance (G/G_{max}) (A) and probability to be open (B) of control or in the presence of 3, 10, and 30 μM allopregnanolone (n = 4–12, ± SD). Solid lines in (B) are the fitting of averaged P_{open} plots with the Boltzmann equation [31]. Normalized conductance is defined as G/G_{max}, where G_{max} is the maximum conductance value at voltages close to 0 mV. The open probability is calculated as $P_{open} = (G-G_{min})/(G_{max}-G_{min})$, where G_{min} is the minimum conductance. (C) Plots of the effective gating charge, n (*left*), and the voltage at which half of the channels are open, V_0 (*right*), calculated by fitting of the P_{open} in individual experiments with the Boltzmann equation (n = 4–12, ± SD). In (C), differences between 3, 10, and 30 μM allopregnanolone and control are non-significant ($p > 0.2$, one-way ANOVA).

Table 1

Summary of residues photolabeled by 5α-6-AziP or KK200 in WT or E73Q mVDAC1. The numbered sites in the left column correspond to the sites previously proposed by docking and MD simulations [14].

	WT-5α-6-AziP	E73Q-5α-6-AziP	WT-KK200
E73 Site	E73	Y62, Y67	F99
Site 1			C127
Site 2/3			G192
Site 4			L245
Site 5			L297